

# Global network design for robust operation of microfluidic droplet generators with pressure-driven flow

Tomasz Glawdel · Carolyn L. Ren

Received: 16 February 2012 / Accepted: 4 April 2012 / Published online: 24 April 2012  
© Springer-Verlag 2012

**Abstract** This study investigates the influence of both local generator design and global network architecture in improving the stability and operational performance of microfluidic droplet generators. We identify naturally occurring short-term and long-term oscillations that are related to changes in the flow of the two phases. Short-term oscillations are related to the creation of each droplet and are quantified by tracking droplet speed in the network. Long-term oscillations are caused by dynamic feedback associated with the periodic change in the hydrodynamic resistance of the network as droplets enter and exit the system. Our analysis identifies that these long-term oscillations are best quantified by measuring changes in droplet spacing rather than the conventional method of using droplet size. Furthermore, we find that these long-term oscillations have a periodicity that matches the residence time of droplets within the network. In combination with experiments, a simple compact model is developed to study these oscillations and guide the network design of droplet generators. As part of this analysis a set of design rules is developed to help improve overall generator performance using pressure-driven flow.

**Keywords** Microfluidics · Droplets · Droplet generators · Two-phase flow · Pressure-driven flow · Stability

---

**Electronic supplementary material** The online version of this article (doi:10.1007/s10404-012-0982-y) contains supplementary material, which is available to authorized users.

---

T. Glawdel · C. L. Ren (✉)  
Department of Mechanical and Mechatronics Engineering,  
University of Waterloo, 200 University Ave W., Waterloo,  
Canada  
e-mail: c3ren@uwaterloo.ca

## 1 Introduction

Droplet generators are typically one part of a larger system of components that are used to manipulate droplets as they traverse a network of microchannels. Because of feedback through the network, each component is coupled together through the pressure field. Consequently, periodic changes in pressure will coincide with periodic changes in flow rate, and thus erratic motion and production of droplets. These fluctuations are caused by variations in the hydrodynamic resistance of the channels and by the growth and collapse of interfaces (van Steijn et al. 2008; Beer et al. 2009; Korczyk et al. 2011). There are several motivations for reducing fluctuations in velocity. Accurate timing of downstream events, such as coalescence, breakup and sorting, depends on steady transport as there is little margin for errors due to the high frequency of droplet production (10 Hz to 10 kHz). Fluctuations in velocity correspond to fluctuations in flow rate. Both the magnitude of flow and the ratio of the dispersed and continuous phase flow rates influence droplet production (Christopher and Anna 2007). Therefore, oscillations in velocity can potentially indicate underlying variation in droplet production (size, spacing and frequency). Clearly reducing these types of variations will improve generator output.

Fluctuations in droplet generation may be classified by the time period over which they occur. Short-term fluctuations occur on a time scale similar to the rate of droplet production as they correspond with the cyclic creation and destruction of the two-phase interface. For instance, van Steijn et al. (2008) observed periodic fluctuations up to 30 % from the average velocity in a gas/liquid T-junction generator. The authors identified the source of these fluctuations as the large pressure burst that occurs when a droplet expands into the exit reservoir. Similar results were

also observed for liquid/liquid generators by Beer et al. (2009). The authors applied a fast Fourier transform (FFT) analysis to the velocity fluctuations and found that the main power spectrum peak matched the droplet generation frequency. In contrast to the observation of van Steijn et al., the authors found that the periodic spike in velocity occurred at the point of neck rupture rather than when a droplet exited the channel.

Long-term oscillations extend over several droplet cycles. These oscillations can be imposed on the system from outside sources or may occur naturally. Syringe pumps are a common culprit of these external fluctuations if they are employed. Generally, syringe pumps suffer from extremely long transient times to reach steady state, especially when small channels are used. Ratcheting of the stepper motor creates pulsatile flow at low revolutions, and imperfections in the drive screw cause slow variations in the flow rate resulting in subsequent variation in droplet generator output (de Mas et al. 2005; Korczyk et al. 2011). Depending on the syringe used, the period of these oscillations can be surprisingly long, up to 30–60 min.

Feedback is more pronounced for systems operating under pressure-driven flow if the microchannel network is not designed properly. Naturally occurring oscillations form because of feedback created by the temporally varying channel resistance. As droplets enter and exit the system they dynamically modify the resistance of channels and by association the flow rates and droplet generation (Ward et al. 2005; Sullivan and Stone 2008; Glawdel et al. 2011). Ward et al. (2005) demonstrated the significant effect that the two different flow types have on the operation of a flow focusing generator operating in the dripping regime. The effect of feedback is even more prevalent in designs where multiple generators are used in parallel. Distribution of oil and water depends on the hydrodynamic resistance of the network which changes with time. Under these conditions, droplet generation can experience several regimes where the generators operate in phase, out of phase, or generation is completely chaotic (Hashimoto et al. 2008; Barbier et al. 2006; Li et al. 2008; Tetradis-Meris et al. 2009).

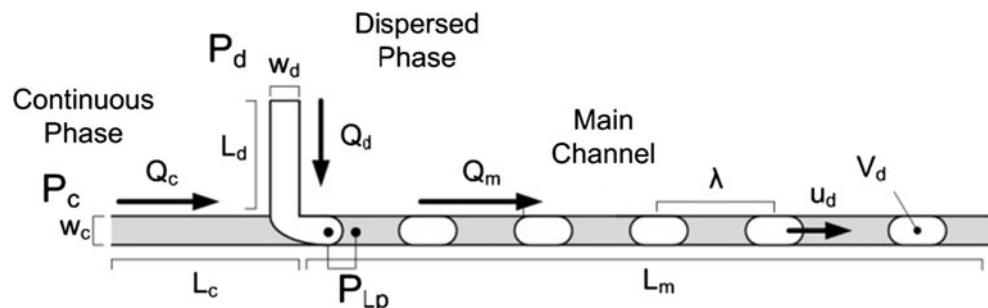
Here, we take a global perspective to investigate the influence of network architecture on the performance of microfluidic droplet generators operating with pressure-driven control. The study focuses on a single droplet generator and the factors which influence variation in droplet size, speed and spacing. The hydrodynamic network is represented by a compact model of the T-junction design. This model is then implemented into a numerical code which couples the two-step generation model with the global flow network conditions. Using this model, contributions of various sources to the fluctuations of droplet size, spacing and speed are studied. As part of this analysis, a set of “design rules” are developed to help improve overall generator performance using pressure-driven flow. The results of these models are confirmed with experimental data with good agreement.

## 2 Compact hydrodynamic model

In this section, a compact model is developed to describe the operation of the T-junction generator. The relevant parameters describing a standard T-junction generator operating under pressure-driven control are presented in Fig. 1. All of the geometric dimensions are outlined except for the height,  $h$ , which is assumed to be uniform throughout the network. The flow rate in the main channel,  $Q_m$ , is the sum of the flow rates of the continuous phase,  $Q_c$  and dispersed phase,  $Q_d$ . Droplets are formed with a volume,  $V_d$ , at a frequency,  $f$ , and spacing,  $\lambda$ , and are transported along the channel at a velocity  $u_d$ . The global network geometry is given by the length of the three channels  $L_c:L_d:L_m$ . The flow of the two phases is controlled by the applied pressures  $P_c$  and  $P_d$ . Additional relationships can be derived for the droplet flow rate,  $Q_d = V_d f$ , droplet velocity,  $u_d = \lambda f$ , and number of droplets in the main channel,  $n = L_m/\lambda$ .

Fluid flow,  $Q$ , and pressure drop,  $\Delta P$ , can be described by the Hagen–Poiseuille relation,  $Q = \Delta P/R_{\text{hyd}}$ . The hydrodynamic resistance of a rectangular microchannel is a non-linear function that scales as  $L/wh^3$  (Bruus 2007).

**Fig. 1** Schematic of the T-junction generator operating under pressure-driven control with the relevant parameters indicated



Using compact hydrodynamic modelling, the non-dimensionalized (marked by \*) pressure and flow fields are:

$$P_j^* = \frac{P_j}{P_c} = \frac{R_d^* + (P_d^* - P_{Lp}^*)}{\frac{R_d^*}{R_m^*} + R_d^* + 1} \quad Q_d^* = \frac{Q_d}{P_c/R_c} = \frac{P_d^* - P_{Lp}^* - P_j^*}{R_d^*}$$

$$Q_c^* = \frac{Q_c}{P_c/R_c} = 1 - P_j^* \quad Q_m^* = \frac{Q_m}{P_c/R_c} = \frac{P_j^*}{R_m^*} \tag{1}$$

All the hydrodynamic resistances are normalized by  $R_c$  and the pressures by  $P_c$ .  $P_j$  is the pressure at the intersection and  $P_{Lp}$  is the Laplace pressure drop across the emerging interface, estimated from the curvature of the interface while inside the dispersed channel  $P_{Lp} = 2\gamma(w_d^{-1} + h^{-1})$  (Malsch et al. 2010; Ward et al. 2005). The resistance of the main channel is the base resistance  $R_{mo}$ , plus the contribution from droplets in the channel  $R_{drop}$ :  $R_m = R_{mo} + nR_{drop}$ . Note that droplet resistance is a complex function that depends on several factors including the viscosity ratio, droplet speed, surface tension, channel geometry, size and spacing of the droplets (Labrot et al. 2009; Vanapalli et al. 2009; Fuerstman et al. 2007). Although several studies have attempted to quantify the influence of these various factors to a certain degree, it still remains difficult to accurately predict droplet resistance for a specific setup without having some empirical data to work with. In the early design process, however, a suitable rule of thumb is that each droplet will increase the resistance of the segment of channel it occupies by 2–5 times.

### 2.1 Working pressure range

For a set of  $P_c$ , the effective range of  $P_d$  is limited to conditions where both phases exit through the main channel. The boundaries of this regime are defined by the cases where the flows change direction in the two inlets ( $Q_c = 0$  or  $Q_d = 0$ ):

$$\frac{R_{mcp}^*}{1 + R_{mcp}^*} + P_{Lp}^* \leq P_d^* \leq \frac{R_d^*}{R_{mdp}^*} + 1 + P_{Lp}^* \tag{2}$$

where  $R_{mcp}^*$  is the resistance when the main channel is filled with the continuous phase and  $R_{mdp}^*$  with the dispersed phase only. Near the lower limit the volume fraction is dominated by the continuous phase (i.e. small droplets with large spacings), while at the upper limit it is dominated by the dispersed phase (i.e. large droplets closely spaced together). The size of this range is of practical significance. If the range is small compared to the resolution of the pressure control system, then droplet production (size, spacing) cannot be finely tuned. Experiments were performed to confirm the validity of Eq. (2) (refer to ESI).

Good agreement was found as measurements were within 2 % of the prediction.

In reality, the available range is often narrower than theoretically predicted by Eq. (2). Usually the pressure is confined to the lower limits because small droplets are often desired rather than long slugs. Furthermore, droplet generation close to the minimum can be very sporadic. The process is as follows. First, a few droplets are formed and they travel down the main channel. The additional droplets increase the resistance of the main channel shifting the lower limit for  $P_d$  upwards. This cuts off the flow of  $Q_d$ , resulting in a pause in the production of droplets until the first droplet leaves the system thereby lowering the limit for  $P_d$  again. The process repeats with a few droplets being formed, followed by a pause, and followed by more droplets again. Generally, one would like to generate a continuous stream of uniform droplets rather than a pulse of highly dispersed droplets. For this to occur, the system has to run slightly above the lower limit predicted in Eq. (2). The number of additional droplets that would cause the flow to stop can be estimated for a pressure  $\delta P_d$  set above the minimum  $P_{dmin}$ :

$$P_{dmin}^* + \delta P_d^* = \frac{R_{mo}^* + nR_{drop}^*}{1 + R_{mo}^* + nR_{drop}^*} + P_{Lp}^* \tag{3}$$

This leads to the following condition which must be met

$$nR_{drop}^* < \frac{\delta P_d^* (1 + R_{mo}^*)^2}{1 - \delta P_d^* (1 + R_{mo}^*)} \tag{4}$$

As long as the number of droplets is less than this limit at the prescribed  $\delta P_d$ , droplets will continuously form without pauses. This calculation is vague without knowing the droplet resistance. However, one can make a reasonable estimate by assuming that, at the lower limit of  $P_d$ , droplets that form will be about as long as the channel width ( $L_{drop} \sim w_c$ ). Droplet resistance thus increases the length of channel it occupies by about two times. Next, one can also assume that droplet spacing will be large near the lower limit, approximately  $\lambda = 20w_c$ , and knowing the main channel length ( $L_m$ ), the number of droplets in the network can be estimated ( $n = L_m/\lambda$ ). This information can then be used to predict  $\delta P_d$ .

### 2.2 Metrics for analysing generation stability

To quantify the stability of generation, both short-term and long-term fluctuations need to be considered. Short-term fluctuations can be quantified by analysing time traces of droplet speed in the main channel. Droplet speed is directly proportional to the flow rate in the main channel,  $Q_m$ , which indicates the cumulative variation in  $Q_d$  and  $Q_c$ . Also of interest is the relative change in the flow rates of

the two phases ( $Q_d$ ,  $Q_c$ ). Fluctuations in the flow ratio ( $\phi = Q_d/Q_c$ ) have a direct consequence as they lead to oscillations in droplet size and spacings. Typically, the stability of microfluidic droplet generators is measured by the polydispersity (size variance) of droplets. Often the exceptional monodispersity of microfluidic droplet generators is quoted to be 1–3 % (Christopher and Anna 2007). However, as will be explained soon, spacing rather than size, is a far more sensitive metric for quantifying long-term fluctuations in performance.

Droplet formation is often described by a two-step model composed of an initial filling stage followed by a necking stage (Garstecki et al. 2006; Steegmans et al. 2009; van Steijn et al. 2010; Glawdel et al. 2012a, b):  $V_d^* = \alpha + \beta\phi$ , where  $V_d^* = V_d/w_c^2h$  is the dimensionless droplet volume and  $\alpha$  and  $\beta$  are parameters corresponding to the two stages. Generally, these two factors can be considered constant for a specific generator geometry and Capillary number, as there is only a weak dependence on variations in flow rate (Christopher et al. 2008). Droplet spacing is also a function of these two parameters:  $\lambda^* = (1 + \phi)(\alpha/\phi + \beta)$  (Glawdel et al. 2012a, b). Using a first order Taylor expansion, fluctuations in flow ratio propagate into relative fluctuations in droplet size and spacing as:

$$\frac{\Delta V_d^*}{V_d^*} = \frac{1}{V_d^*} \left( \frac{dV_d^*}{d\phi} \right) \Delta\phi = \frac{\beta}{\alpha + \beta\phi} \Delta\phi \quad (5)$$

$$\frac{\Delta \lambda^*}{\lambda^*} = \frac{1}{\lambda^*} \left( \frac{d\lambda^*}{d\phi} \right) \Delta\phi = \frac{-\frac{\alpha}{\phi^2} + \beta}{(1 + \phi)\left(\frac{\alpha}{\phi} + \beta\right)} \Delta\phi. \quad (6)$$

Consider a nominal case for a T-junction generator where  $\alpha = 1$ ,  $\beta = 1$  and a flow ratio of  $\phi = 1/10$ , then a 10 % fluctuation in the flow rate ratio results in a droplet volume change of only  $\sim 1$  % but a spacing fluctuation of  $\sim 8$  %. In addition, the 1 % change in volume may only represent a tiny change in droplet length ( $\sim 1$   $\mu\text{m}$ ) which is difficult to measure accurately from video analysis; this is in contrast to spacing changes which are much larger ( $\sim 20$ – $100$   $\mu\text{m}$ ) and thus easier to measure.

Figure 2 plots the expected variance for different flow conditions assuming a 10 % relative fluctuation in the flow ratio. As evidenced in Fig. 2, when small droplets are formed ( $\phi < 0.25$ ), spacing variations are about 3–4 times larger than droplet size variations. This reverses above  $\phi = 0.5$  where droplets size becomes more sensitive to fluctuations (droplets are bigger than spacing). Therefore, in the range of practical significance (i.e. lower  $\phi$ ), spacing is a far more sensitive indicator to the stability of the system than droplet size. One can also surmise that a low variance in spacing results in any even lower variance in droplet size in this range. Furthermore, measuring spacing fluctuations compliments measurements of droplet velocity

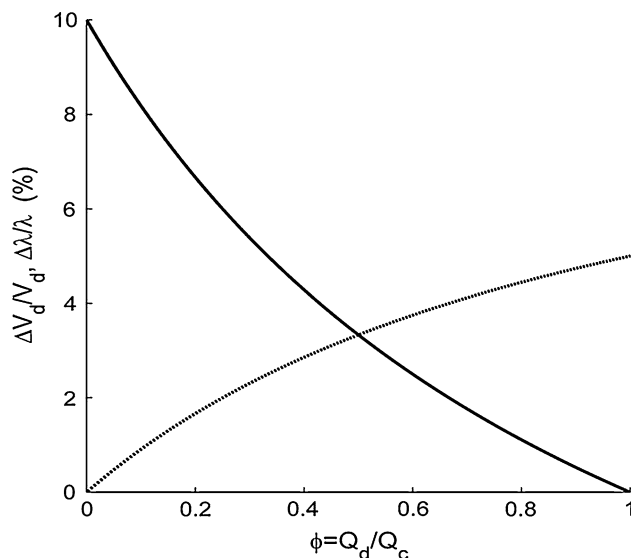


**Fig. 2** Plot of the deviation in droplet volume (*dotted line*) and spacing (*solid line*) against the flow ratio under the conditions of  $\alpha = 1$ ,  $\beta = 1$  and 10 % fluctuations of  $\phi$ . Calculations are made using Eqs. (5–6)

as these fluctuations appear over the short term (1 cycle), while spacing fluctuations appear over the long term (10–1,000 cycles). For proper assessment of the system, measurements should be made on both scales to accurately quantify the stability of the generator.

### 3 Experimental

Experiments were performed with three different oil/surfactant combinations (silicon oil, hexadecane, FC-40) using water/glycerol as the dispersed phase, with the viscosity ratio varying from  $\mu_d/\mu_c = 0.1, 0.2, 0.33, 0.5$ , the intersection geometry from  $w_d/w_c = 0.33, 0.5, 1$ , the height from  $h/w_c = 0.15, 0.35, 0.5$  with global architecture of  $L_c:L_d:L_m$  (1:1:5, 5:1:2, 1:5:2 cm) and Capillary numbers from  $Ca = 0.001 \rightarrow 0.022$ . Chips were fabricated in PDMS (polydimethylsiloxane) using standard soft lithography techniques. PDMS molds were bonded to PDMS-coated glass slides to create homogenous microchannels. Fluids were controlled using a high precision microfluidic pressure system (MSFC 8C, Fluigent) that operates up to 1 bar. Chips were mounted on a microscope (Eclipse Ti, Nikon) and videos of the droplets were recorded using a high speed camera (V-210, Vision Research). A custom program written in Matlab (Mathworks) was used to extract the size, speed and spacing of droplets from the videos. Specific experimental details are provided in Supplementary Information (ESI).

### 4 Results and discussion

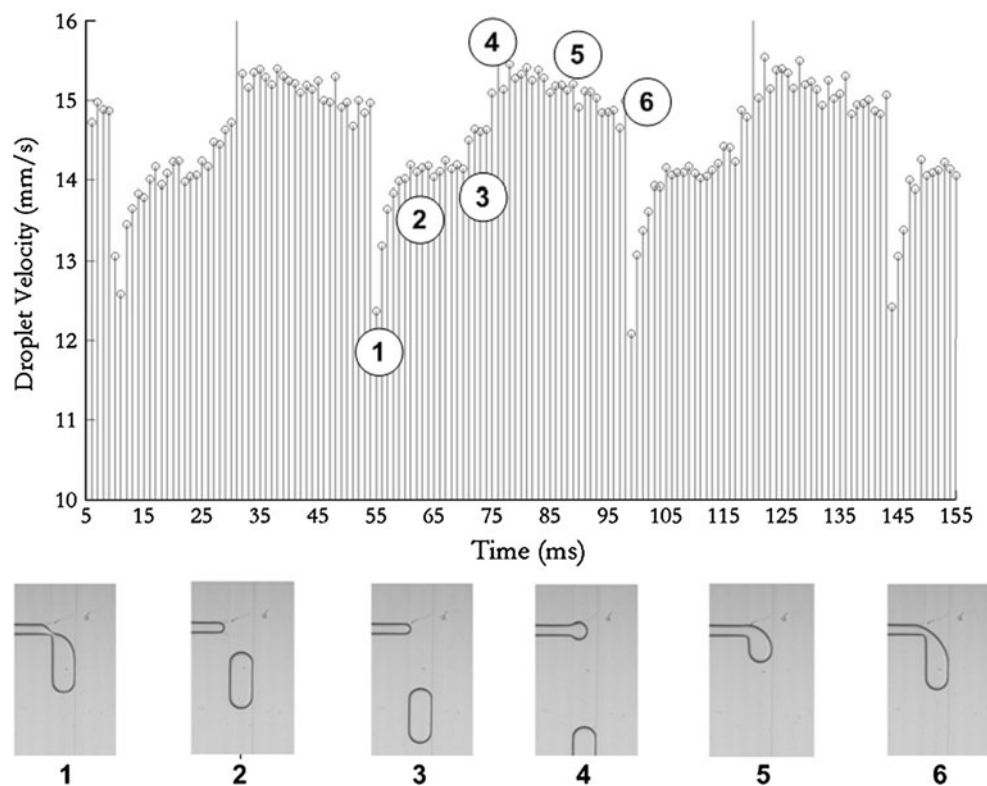
As mentioned before, short-term fluctuations have a period of oscillation close to the droplet generation frequency. These fluctuations are related to the creation and destruction of the two-phase interface. Figure 3 shows an experimental data set with periodic velocity fluctuations up to ~20 %. Measurements were made by tracking the displacement of a recently formed droplet just downstream from the T-junction generator. Velocity fluctuations are highly repeatable over each droplet formation cycle. In this example, the velocity fluctuation occurring at the T-junction generator is caused by the dynamically changing Laplace pressure drop. Comparing the velocity profile with the formation process occurring upstream, changes in velocity coincide with different stages of the formation process number 1 through 6 in Fig. 3:

- Droplet pinch-off coincides with a reversal of oil flow from the tip of the droplet into the neck region (van Steijn et al. 2009). This causes a severe drop in velocity as the contribution of  $Q_c$  to  $Q_m$  decreases. After the droplet detaches the interface retracts into the side channel to a distance of  $w_d$  from the intersection.
- The interface quickly recovers from 1 → 2, and the velocity increases slightly; however, it is below the maximum velocity seen later when the interface penetrates into the main channel. This is because the curvature of the interface is higher in the side channel

which results in a larger Laplace pressure drop across the interface. Generally, the difference between the two plateaus 2 → 3 and 4 → 5 was more significant when the intersection design was asymmetric ( $w_d:w_c = 1:2, 1:3$ ) and less when it was symmetric (1:1).

- Afterwards (2 → 3) the interface begins to advance within the dispersed phase channel until it reaches the entrance into the main channel. During the advancement the curvature remains approximately the same ( $2/w_d$ ), and thus  $Q_m$  is approximately constant throughout this stage.
- Once the interface reaches the main channel it begins to expand, decreasing the curvature and the Laplace pressure drop across the interface causing an increase in the contribution of  $Q_d$ . The maximum velocity occurs at 4, which may be a surprise, since it happens before the interface expands to its maximum size ( $2/w_c$ ). Presumably this is caused by the fact that the gap between the wall and interface closes, which blocks the flow of the continuous phase thereby decreasing the contribution of  $Q_c$  to  $Q_m$  (Christopher et al. 2008; Garstecki et al. 2006; Glawdel et al. 2012a, b).
- From 4 → 5→6 the velocity decreases slightly as the pressure drop across the drop changes. Presumably there are two contributions to the decrease. As the droplet increases in length, the amount of  $Q_c$  flowing through the gutters decreases due to the increase in hydrodynamic resistance. Secondly, as the neck is

**Fig. 3** Velocity of a droplet that is downstream of the T-junction generator for hexadecane and water,  $L_c:L_d:L_m = 1:1:5$  cm,  $w_d = 50 \mu\text{m}$ ,  $w_c = 100 \mu\text{m}$ ,  $h = 35 \mu\text{m}$ . The velocity varies significantly over a droplet formation cycle, and in this case the standard deviation is >5 %. The velocity fluctuations correspond to different stages of the formation cycle, as indicated by the numbered images. The formation cycle is approximately 45 ms long and images were taken at 1,000 fps



thinning the change in curvature between the front and back of the droplet is causing the pressure drop across the droplet to decrease, lowering the flow of  $Q_c$ . This finally culminates in the sudden collapse of the neck at 6 and the sharp decrease in  $Q_m$ .

Unlike van Steijn et al. (2008) the spike in velocity caused by a droplet leaving the channel was not observed in this example. This, however, does not completely eliminate the possibility of fluctuations still occurring at the outlet given that the flexibility of PDMS may attenuate these fluctuations before they reach the generator where observations were made.

#### 4.1 Scaling analysis of velocity fluctuations

A scaling analysis may be performed to predict the order of magnitude of velocity fluctuations. This may be accomplished by calculating the relative fluctuation of  $Q_m$  due to perturbations in certain variables. Three primary sources for these fluctuations are considered: (1) Laplace pressure fluctuations caused by the evolving interface at the generator. Here only the expansion of the interface from the dispersed phase inlet to the main channel is considered. (2) Oscillations in the input pressures  $P_d$  and  $P_c$ . The main source of these oscillations would be the feedback control in the pressure regulation system. (3) Oscillations in the resistance of the main channel as droplets enter or leave the network. This is modelled by the addition or subtraction of a single drop  $\delta R_m = R_{\text{drop}}$ . Note that this does not include the sudden pressure pulse created by a droplet expanding uncontrolled into the exit reservoir.

Using a first order Taylor expansion, Laplace pressure fluctuations propagate into relative velocity fluctuations as:

$$\frac{\Delta u_d}{u_d} \Big|_{P_{Lp}} \propto \frac{1}{Q_m^*} \left( \frac{dQ_m^*}{dP_{Lp}^*} \right) \Delta P = \frac{\Delta P_{Lp}^*}{R_d^* + P_d^* - P_{Lp}^*}. \tag{7}$$

The Laplace pressure change is calculated by estimating the change in interface curvature from the inlet of the dispersed channel ( $\kappa = 2/w_d + 2/h$ ) into the main channel ( $\kappa = 2/h$ ):  $\Delta P_{Lp}^* = 2\gamma w_d^{-1} P_c^{-1}$ . Fluctuations in the input pressures  $\Delta P_d^*$  can also cause droplet velocity oscillations:

$$\frac{\Delta u_d}{u_d} \Big|_{P_d} = \frac{\Delta P_d^*}{R_d^* + P_d^* - P_{Lp}^*}. \tag{8}$$

Similarly, fluctuations caused by a single droplet leaving the channel can be calculated as:

$$\frac{\Delta u_d}{u_d} \Big|_{R_m} = \frac{R_{\text{drop}}^*}{R_m^*} \frac{(R_d^* + 1)}{R_d^*/R_m^* + R_d^* + 1} \tag{9}$$

The total velocity fluctuation may then be calculated as the vector sum:

$$\frac{\Delta u_d}{u_d} = \left( \left( \frac{\Delta u_d}{u_d} \Big|_{P_{Lp}} \right)^2 + \left( \frac{\Delta u_d}{u_d} \Big|_{R_m} \right)^2 + \left( \frac{\Delta u_d}{u_d} \Big|_{P_d} \right)^2 \right)^{1/2} \tag{10}$$

Figure 4 plots the predicted velocity fluctuations with the measured values  $\sigma(u_d)/u_d$  from experiments. From the experiments, the standard deviation  $\sigma(u_d)/u_d$  is used as a metric for comparison. Open circles correspond to experiments without surfactants and filled circles with surfactants, the solid line represents perfect correlation between the experimental and predict values. The data show that the two measures scale together and that the analysis is successful in predicting the order of magnitude of the velocity fluctuations. Generally, the prediction slightly underestimates the real fluctuations; the reason being the omission of several additional sources of fluctuations, namely droplet pinch-off and uncontrolled droplet expansion.

Velocity fluctuations are generally much lower when surfactants are added to the system. Surfactants lower the surface tension which has a twofold effect: (1) it reduces the Laplace drop at the interface near the T-junction nullifying the influence of the expansion and necking pulses and (2) it reduces the hydrodynamic resistance of a droplet by lowering the contribution of the front and end caps during transport and expansion (van Steijn et al. 2008). The good agreement between the predictions put forth by the compact model and the experiments provide a certain degree of validation for using compact modelling to describe the overall performance of the generator.

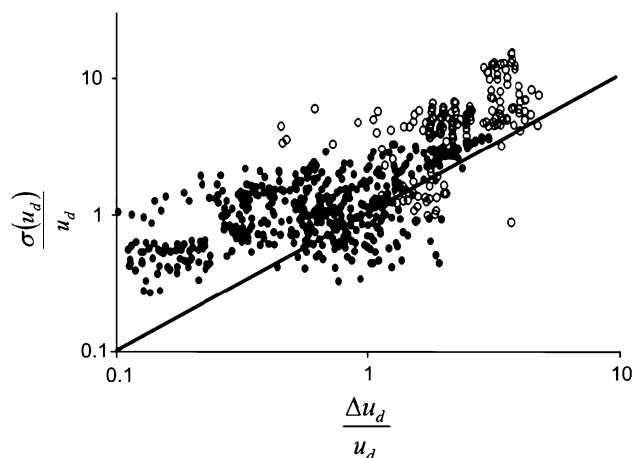


**Fig. 4** Relative velocity fluctuations observed experimentally compared to the prediction of Eq. (10). Data are shown on a log-log plot in terms of percentages. *Closed circle* corresponds to experiments using surfactants and *open circle* to those without. The *solid line* represents perfect parity

### 4.2 Analysis of spacing fluctuations

Typical results of the time-dependent spacing output of a droplet generator are presented in Fig. 5. Droplet spacing experiences both short-term and long-term oscillations. Short-term oscillations are created by the stochastic nature of the break up process and other sudden pulses such as a droplet exiting a channel. However, from within the noise created by the short-term fluctuations, a natural steady and repeatable long-term signal can be seen (smoothed line in Fig. 5). Analysis shows that these oscillations have a period that coincides with the time it takes to completely replace the droplets within the channel, i.e.  $\tau = n_{\text{drop}}$ . This period may also be interpreted as the average residence time of a droplet in the main channel. The underlying cause of these long-term oscillations is the dynamically changing contribution of droplet resistance to  $R_m$  as the flow rates vary slightly over time. If oscillations exist then each droplet has a unique size and corresponding hydrodynamic resistance that contributes to the overall channel resistance and the flow of the two phases. Once a droplet is formed it influences the formation of all subsequent droplets, while it remains within the channel. Thus, long-term oscillations are associated with the residence time of the droplets in the outlet, which can also be thought of as the number of subsequent droplets that are influenced by a newly formed droplet.

To confirm this observation, the data were analysed using fast Fourier transfer (FFT) analysis in order to extract the strongest frequency prevalent in the spacing data. Figure 6 presents FFT results for the experiments in Fig. 5. The strongest peak appears at a cycle time  $\tau/n_{\text{drop}} \sim 1$  indicating that main oscillations have a cycle that equals the channel volume replacement time. Analysis of other experimental results confirms power spectrum significant

peaks near  $\tau/n_{\text{drop}} \sim 1$  and/or at the next harmonic  $\tau/n_{\text{drop}} \sim 0.5$ . A similar correlation between droplet residence time and cyclic behaviour is also seen in sorting of droplets at a simple junction (Sessoms et al. 2010; Glawdel et al. 2011). Sorting patterns form due to dynamic feedback of decisions made by droplets which have a lifetime associated with the time they remain in the channel.

### 4.3 Compact numerical model of drop formation

To further investigate this phenomenon a simple compact numerical model was developed for the droplet generation process (Cybulski and Garstecki 2010; Sullivan and Stone 2008; Schindler and Ajdari 2008). In these models droplets are treated as point particles and microchannels can be reduced to 1-D pipe networks. At each time step the flow

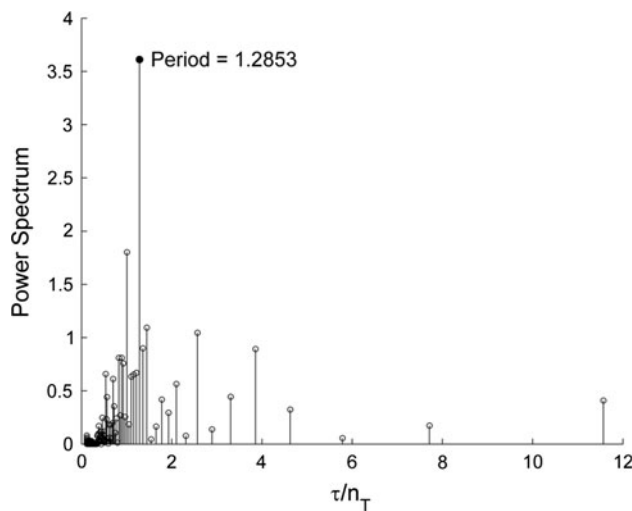
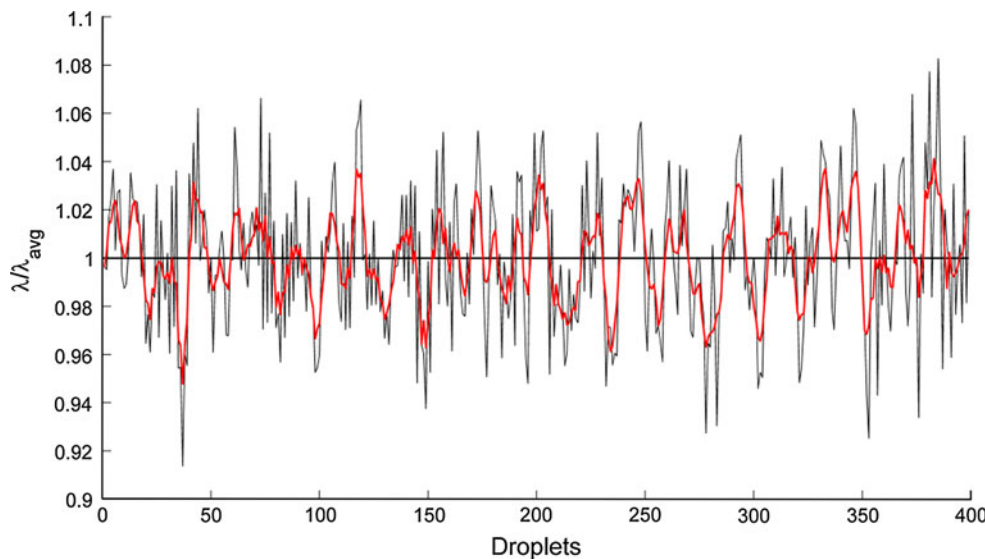


**Fig. 6** Power spectrum of the fast Fourier transform of data in Fig. 5. The strongest peak coincides with the residence time of the droplets

**Fig. 5** Measurement of droplet spacing in a T-junction generator after 10 min of operation. Conditions are for silicon oil and water without surfactant,  $R_c:R_d:R_m = 1:0.5:2$  cm,  $h = 27 \mu\text{m}$ ,  $P_c = 350$  mBar,  $P_d = 355$  mBar. Solid black line is the measured value; red line is a 5-point smoothing average



field and pressure field are calculated using the hydrodynamic model of Eq. (1), where  $R_m$  varies as the number of droplets in the channel changes. We couple the hydrodynamic model of the network with a model for drop formation described by Glawdel et al. (2012a, b). This model divides the formation process into three phases, lag, filling and necking which are described by the scaling relation:  $V_d^* = \alpha_{\text{lag}} + \alpha_{\text{fill}} + \beta\phi$ . To mimic the velocity fluctuation caused by the changes in Laplace pressure in Fig. 3, we set the interface curvature as follows in the three phases:

1. Lag stage: the interface is contained within the side channel after droplet detachment and must move a distance  $w_d$  before entering the counter-flowing continuous stream. Interface curvature is fixed at:  $\kappa = 2/w_d + 2/h$  following the plateau at stage 2  $\rightarrow$  4 in Fig. 3.
2. Fill stage: the droplet expands to fill an initial size  $V_{\text{fill}} = \alpha \cdot w_c^2 h$  prior to necking. Interface curvature in this stage is calculated as:  $\kappa = 2/h$ , following the jump to stage 4.
3. Necking stage: the necking begins and the oil replaces a volume of  $V_{\text{neck}} = \beta \cdot w_c^2 h$ . Interface curvature is estimated as:  $\kappa = 2/h$ , following the relatively stable plateau from stage 4  $\rightarrow$  6.

A highly variable time-stepping algorithm was employed to speed up the simulation. The new time step was calculated as the minimal interval for one of the following events to occur based on the settings in the previous time step:

1. If in phase 1. The time remaining for the interface to cover the distance  $w_d$  inside the dispersed channel inlet:  $\Delta t = w_d / (Q_d w_d h)$ .
2. If in phase 2. The time remaining to reach the final fill volume:  $\Delta t = (V_{\text{fill}} - V_d^{(i)}) / Q_d$ .
3. If in phase 3. The time remaining to reach the final neck volume:  $\Delta t = (V_{\text{neck}} - V_o^{(i)}) / Q_c$ .
4. Time remaining for a droplet to reach the exit.

Each newly formed droplet is placed at the entrance of the main channel and its position is tracked as it travels down the main channel. The size of the droplet is calculated as the amount of  $Q_d$  pumped into the droplet during the three phases. Droplet resistance was then correlated to droplet size by  $R_{\text{drop}} = G_c V_d$ , where  $G_c$  is a conversion factor relating the volume of the droplet to the added resistance. Therefore, each newly formed droplet has a unique volume, resistance and the period of formation. At the end of each time step droplets were transported down the channel a distance of  $\Delta x = \Delta t Q_m / A$ . If a droplet

reached the exit it was removed from the system. Simulations begin with the main channel empty and run for a specified time. In some instances zero-mean random noise was applied to  $P_c$ ,  $P_d$  at each time step. Time traces were recorded for all relevant variables including droplet size, spacing and frequency of the formation.

#### 4.4 Numerical model results

Figure 7 presents the spacing time-trace with the added noise ( $\sigma(P_{d,c}) = 0.25$  mBar) under the same experimental settings in Fig. 5. FFT analysis of the signal confirms that the oscillations in spacing have a period matching closely to the residence time of droplets in the channel,  $\tau/n_{\text{drop}} \sim 1$ . Both the magnitude and period of the oscillations are qualitatively in agreement.

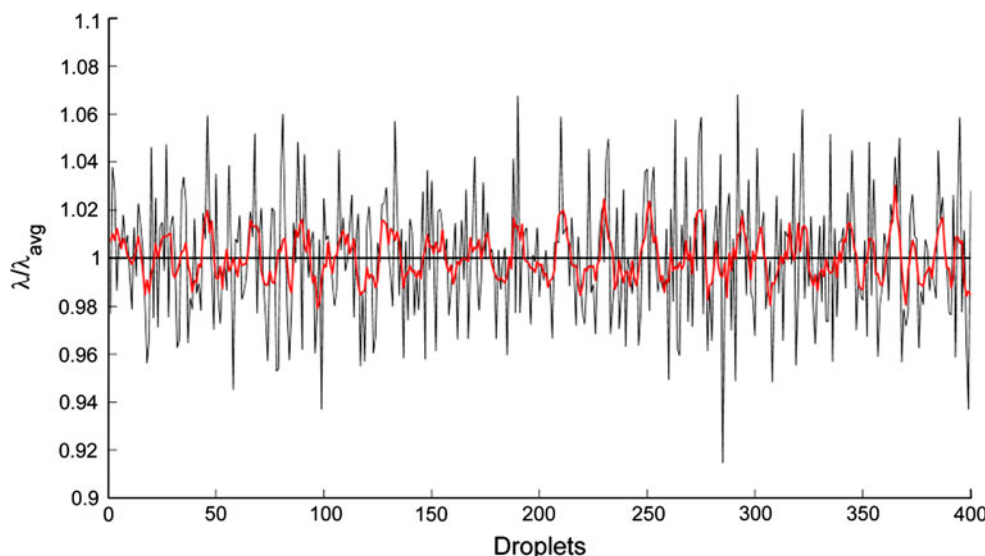
If noise is absent, and the simulation is run for a long-enough time, oscillations eventually subside to a constant output in droplet spacing (see ESI). However, in the presence of noise, the system continues to oscillate even after 100 channel volume replacements. This of course is somewhat expected because of the random perturbations in the inlets ( $P_d$ ,  $P_c$ ), what is interesting, however, is that  $\tau/n_{\text{drop}} \sim 1$  still remains one of the strongest frequencies in the FFT analysis. This suggests that small perturbation caused by the randomness of the input conditions perpetuates the slowly varying oscillations in the system. One may thus conclude that long-term oscillations are expected to always be part of the response of the pressure-controlled droplet generator where feedback is present.

Experiments were also performed to study the transient response during start-up (different than the steady-state response in Fig. 5). Pressures were adjusted so that the interface was just inside the side channel and the main channel was free of droplets. Next,  $P_d$  was increased to a new setting and droplets began to form. A video was recorded of the start up. The time-trace of the spacing is shown in Fig. 8. Again the period of these oscillations closely resembles  $\tau/n_{\text{drop}} \sim 1$ . The initial exponential decay takes about 5 cycles before dampening out to the steady-state response.

Overall, these results are also in agreement with the work of Sullivan and Stone (2008) and their analysis of the effect of feedback on a bubble flow focusing generator. The authors performed a similar numerical simulation and found that the frequency of formation also followed a decaying sinusoidal response. An approximate analytical model developed found that the frequency of formation takes the form:  $f = f_o + A e^{(i-\Delta)\omega t}$ , where  $f_o$  is the steady-state solution,  $A$  the amplitude of the oscillations and  $\omega$  is



**Fig. 7** Measurements of droplet spacing produced by the numerical simulations for conditions similar to the experimental results of Fig. 5: time-trace of droplet spacing. The *solid black line* is the measured values; *red line* is a 5-point smoothing average



the frequency. This sinusoidal response is clearly evident in the numerical and experimental results presented in our study.

#### 4.5 Reducing fluctuations through network design

Here, an analysis is performed to guide design and provide a quantifiable estimation of expected fluctuations in (1) velocity and (2) droplet spacing. The parameters that best capture these two considerations are the flow ratio and the total flow rate in the main channel. Estimates for fluctuations in the total flow rate are provided in Eqs. (7–10). Relative changes in the flow ratio due to the three most prominent sources of variance are:

$$\left. \frac{\Delta\varphi}{\varphi} \right|_{P_{Lp}} = \frac{\Delta P_{Lp} (R_d^* + R_d^* R_m^* + R_d^*)}{(R_m^* + (1 + R_m^*) (P_d^* - P_{Lp}^*)) (R_d^* + R_m^* - R_m^* (P_d^* - P_{Lp}^*))} \tag{11}$$

$$\left. \frac{\Delta\varphi}{\varphi} \right|_{P_d} = \frac{\Delta P_d (R_d^* + R_d^* R_m^* + R_d^*)}{(R_m^* + (1 + R_m^*) (P_d^* - P_{Lp}^*)) (R_d^* + R_m^* - R_m^* (P_d^* - P_{Lp}^*))} \tag{12}$$

$$\left. \frac{\Delta\varphi}{\varphi} \right|_{R_m} = \frac{R_{drop}^* (R_d^* + P_d^* - P_{Lp}^*) (P_d^* - P_{Lp}^* - 1)}{(R_m^* + (1 + R_m^*) (P_d^* - P_{Lp}^*)) (R_d^* + R_m^* - R_m^* (P_d^* - P_{Lp}^*))} \tag{13}$$

The total estimated fluctuation is the vector sum

$$\frac{\Delta\varphi}{\varphi} = \left( \left( \left. \frac{\Delta\varphi}{\varphi} \right|_{P_{Lp}} \right)^2 + \left( \left. \frac{\Delta\varphi}{\varphi} \right|_{R_m} \right)^2 + \left( \left. \frac{\Delta\varphi}{\varphi} \right|_{P_d} \right)^2 \right)^{1/2} \tag{14}$$

Figure 9 plots the average of the flow ratio (Eq. 14) and total flow rate (Eq. 10) variations for different network geometries ( $R_d^*, R_m^*$ ) for standard microchannel sizes ( $w = 100 \mu\text{m}$ ,

$h = 50 \mu\text{m}$ ) under nominal conditions:  $P_c = 500 \text{ mBar}$ ,  $\Delta P_d = 0.5 \text{ mBar}$ ,  $\gamma = 50 \text{ mN/m}$ , and  $L_{drop} = 150 \mu\text{m}$ . These calculations are made for a fixed flow ratio  $\varphi = 0.3$  and for two continuous channel lengths  $L_c = 5, 10 \text{ mm}$ . Fluctuations are less than 5 % in the area bounded by the thick black line in the figure. Analysis of additional parametric combinations reveals that, in general, fluctuations are reduced when  $R_d > R_m > R_c$ . As well, lower droplet resistance and interfacial tension decrease variance as expected.

#### 4.6 Design guidelines

From the analysis presented above, a set of design rules can be devised with the focus of (1) minimizing fluctuations in

droplet velocity, size and spacing, and (2) maximizing the working range to increase the control over droplet generation. Comments are provided in point form below:

##### 4.6.1 Surfactants

Surfactants should be used whenever possible as they combine to reduce  $P_{Lp}$ ,  $R_{drop}$ , and any effect involving distortion of droplet shape (exit expansion). Adding

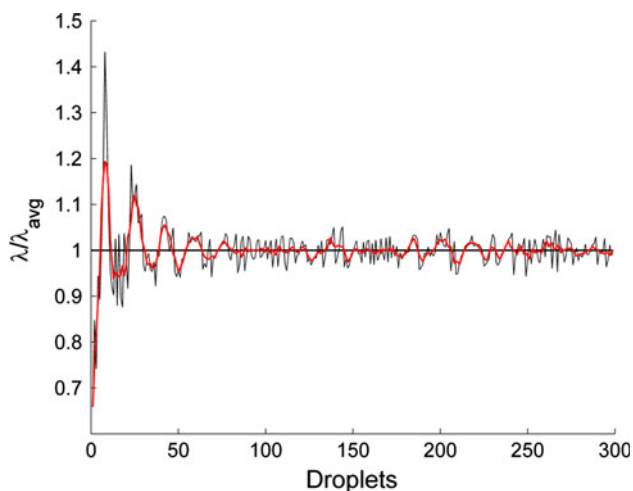


**Fig. 8** Experimental results for the start-up response of a T-junction generator. Conditions are for silicon oil and water without surfactant with a network design of  $R_c^* : R_d^* : R_m^* = 1 : 0.5 : 2$ ,  $h = 50 \mu\text{m}$ , and  $P_c = 300 \text{ mBar}$

surfactants is the most effective means of reducing variance in droplet production.

#### 4.6.2 Local generator geometry

If surfactants cannot be added then the generator intersection should be designed to minimize expansion of the interface. For T-junction generators this means using a 1:1 ( $w_d:w_c$ ) designs. The exit should be constructed in some way to reduce pressure spikes that are associated with droplet expansion. For a fixed pressure  $P_c$ , increasing the height reduces fluctuations because the Laplace pressure drop decreases.

#### 4.6.3 Global network configuration

The number of droplets should be large and the resistance of one droplet compared to the main channel resistance,  $R_{\text{drop}}/R_m$ , should be small to minimize the influence of a single droplet leaving the channel,  $R_d \ll R_{\text{mo}} + nR_{\text{drop}}$ . A reasonable suggestion is that the main channel should hold at least 50 droplets with a spacing  $\lambda = 10w_c$ , so that fluctuations in  $R_m$  will be around 1%. For the network design, following condition should be met  $R_d > R_m > R_c$ . This means a relatively short inlet for the continuous phase and a very long inlet for the dispersed phase.

The other option is to make the two inlet channels very resistive compared to the outlet ( $R_c \gg R_m$  and  $R_d \gg R_m$ ). However, this option is less favourable as it limits the production rate of droplets. Generally, the flow of the continuous phase is 5–10 times greater than the dispersed phase. A long inlet for the continuous phase means that excessively high pressures are needed to generate a

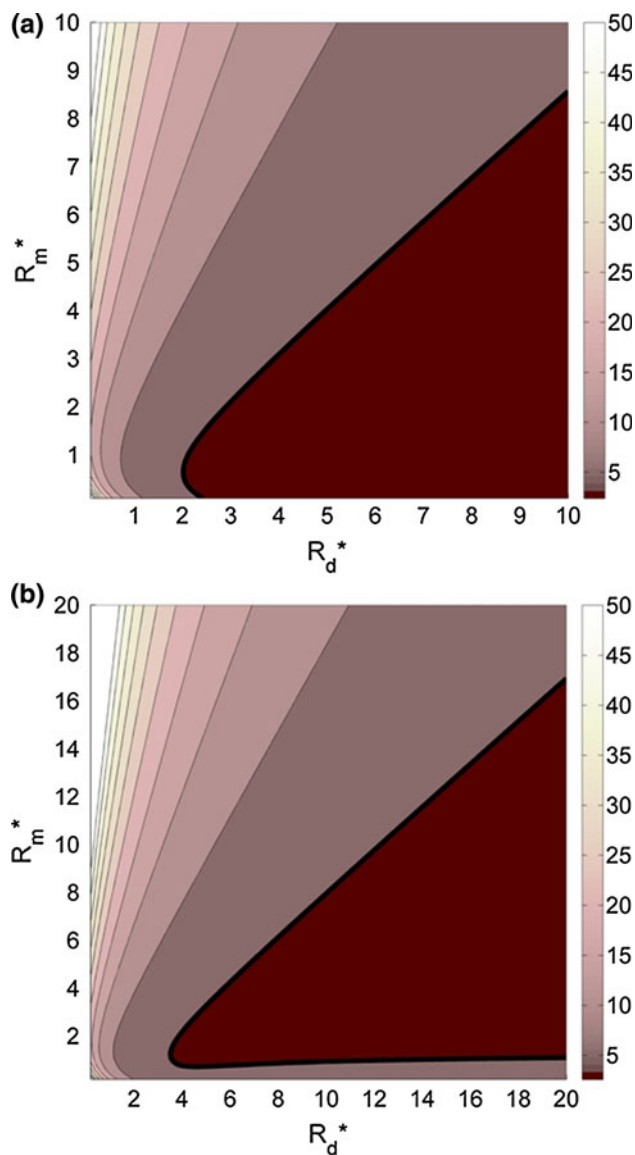


**Fig. 9** Contour plots of the average variance (flow ratio and total flow rate) (%) from all three sources versus the global network geometry. **a**  $\Delta P_{\text{Lp}}^* = 0.06$ ,  $\Delta P_d^* = 0.001$ ,  $R_{\text{drop}}^* = 0.05$ . **b**  $\Delta P_{\text{Lp}}^* = 0.06$ ,  $\Delta P_d^* = 0.001$ ,  $R_{\text{drop}}^* = 0.1$

significant amount of flow since most of the pressure drop is contained in the long inlet channel. Higher pressures require more bulky equipment and increase the chance of leakage.

A reasonable design criteria is that  $R_d = R_m$  since improvements are marginal for  $R_d > R_m$ . Remember the hydrodynamic resistance depends on the viscosity of the fluid. For most water/oil combinations  $\mu_d/\mu_c = 1/3 \rightarrow 1/10$ , and for a design with uniform cross-section the dispersed channel will need to be 3–10 times longer than the main channel. For bubble generation where air is the dispersed phase, this means excessively long inlet channels, in the range of several meters, to compensate for the low

viscosity. The necessity of these long channels for stable bubble generation has been known for quite some time (de Mas et al. 2005).

#### 4.6.4 Pressure system

For the condition where  $R_d = R_c$ , the effective pressure range is  $P_{dmin} < P_d < 2P_c$ . A highly stable and reliable source of air pressure is required to eliminate transients in the air supply. As part of this system, high-resolution pressure regulators are needed to fine tune the flow of the two fluids. For a given  $P_c$  and pressure resolution, one should verify that the resolution available for controlling droplet size and spacing is sufficient for the application by calculating the number of discrete operating points available.

Overall, higher applied pressures ( $P_c$ ) improve stability by (1) reducing the relative importance of Laplace pressure drop ( $P_{Lp}$ ) compared to hydrodynamic pressure drop (2) reducing droplet resistance as  $R_{drop} \propto u_{drop}^{-1/3}$  and droplet speed is proportional to the applied pressure (Bretherton 1961) (3) wider dynamic range for the  $P_d$  when compared to the resolution of the pressure regulator and (4) reducing the effect of external pressure fluctuations that may occur such as changes in head between reservoirs as fluid levels rise and fall during operation. Running the system away from  $P_{dmin}$  also reduces fluctuations as the majority of the pressure drop in the dispersed channel ( $P_d - P_{Lp} - P_j$ ) is from hydrodynamic losses and not pressure jump across the interface  $P_{Lp}$ . For the readers' reference, a case study is presented in the ESI to provide some context for these rules.

#### 4.7 Testing of design rules

Figure 10 plots  $\sigma(\lambda)/\lambda$  against the dispersed pressure  $P_d$  for three network designs ( $R_c^* : R_d^* : R_m^*$ ): 1:4:5, 1:0.7:5, 1:0.1:5 and recording the spacing of at least 3,000 droplets. The data confirm many of the conclusions drawn from the analysis of reducing fluctuations in  $P_j^*$  (Eq. 11). As expected, spacing fluctuations decrease with increasing  $P_c$  as the effects of  $P_{Lp}$  diminishes. On average, fluctuations decreased in accordance with the design rules outlined for the global network ( $\uparrow R_d$  causes  $\downarrow \sigma(\lambda)/\lambda$ ). From the figure, the stability (lowest to highest variance) of the three designs can be ordered as (open circle) 1:4:5, (unfilled triangle) 1:0.7:5 and (filled rectangle) 1:0.1:5, in agreement with theory. Furthermore, moving the system away from  $P_{dmin}$ , by increasing  $P_d$ , also increases the stability of the system as highlighted by the arrow in Fig. 10, again in agreement with theory. These results also demonstrate the impressive performance which can be achieved by following the design rules. Less than 0.5 % variance in

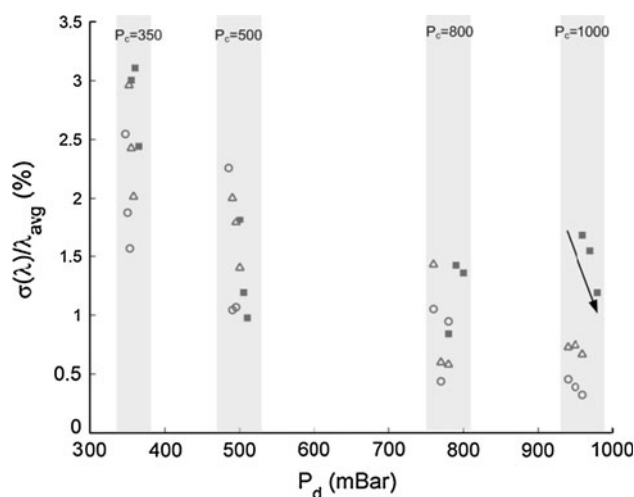


**Fig. 10** Measured variance in droplet spacing for different network designs as a function of applied pressure  $P_d$ . Data correspond to a (1:1) T-junction intersection with network geometries of  $R_c^* : R_d^* : R_m^*$ : open circle 1:4:5, unfilled triangle 1:0.7:5 and filled rectangle 1:0.1:5

spacing was achieved for the 1:4:5 design and less than 1 % variance for the 1:0.7:5 design at the upper end of  $P_d$ . Both of these results would correspond to  $<1$  % variance in droplet size.

### 5 Conclusions

This work has furthered the understanding of the influence of global network design on the behaviour of pressure-driven microfluidic droplet generators. In this work, we have shown that fluctuations can be characterized by two time scales: short-term fluctuations occur over a period equal to, or less than, the droplet generation period; and long-term fluctuations extend over several droplet generation cycles. The effect of these two fluctuations can be quantified by monitoring the droplet velocity (short-term) and droplet spacing (long-term).

Both types of fluctuations can be minimized through effective design of the droplet generator. Short-term fluctuations are typically prevalent when there are significant changes in interface curvature and large surface tension. Minimizing deviations in interface shape using a 1:1 design and taper outlet is an effective means of reducing fluctuations. Long-term fluctuations occur because of the feedback effect between the flow field and the production of droplets. These fluctuations tend to have a periodicity that is associated with the life-time of a droplet in the system. Long-term fluctuations cannot be entirely eliminated, but their influence can be subdued through proper design of the global network as identified by the simple theoretical model which was developed as part of this study. Constant flow conditions can be achieved even with the use of

pressure-driven flow through proper design of the global network architecture which should enhance the long-term production of monodispersed droplets.

**Acknowledgments** The authors gratefully acknowledge the support from the Natural Sciences and Engineering Research Council of Canada, Canada Foundation for Innovation of Canada, International Science and Technology Program of Canada and Ontario Centers of Excellence to Dr. Carolyn Ren through her grants, and the Canada Graduate Scholarship to Tomasz Glowdel.

## References

- Barbier V, Willaime H et al (2006) Producing droplets in parallel microfluidic systems. *Phys Rev E* 74(4):046306
- Beer NR, Rose KA et al (2009) Observed velocity fluctuations in monodisperse droplet generators. *Lab Chip* 9(6):838–840
- Bretherton FP (1961) The motion of long bubbles in tubes. *J Fluid Mech* 10(2):166–188
- Bruus H (2007) *Theoretical microfluidics*. Oxford University Press, New York
- Christopher GF, Anna SL (2007) Microfluidic methods for generating continuous droplet streams. *J Phys D* 40(19):R319–R336
- Christopher GF, Noharuddin NN et al (2008) Experimental observations of the squeezing-to-dripping transition in T-shaped microfluidic junctions. *Phys Rev E* 78(3):036317
- Cybulski O, Garstecki P (2010) Dynamic memory in a microfluidic system of droplets traveling through a simple network of microchannels. *Lab Chip* 10(4):484–493
- de Mas N, Gunther A et al (2005) Scaled-out multilayer gas-liquid microreactor with integrated velocimetry sensors. *Ind Eng Chem* 44(24):8997–9013
- Fuerstman MJ, Lai A et al (2007) The pressure drop along rectangular microchannels containing bubbles. *Lab Chip* 7(11):1479–1489
- Garstecki P, Fuerstman MJ et al (2006) Formation of droplets and bubbles in a microfluidic T-junction—scaling and mechanism of break-up. *Lab Chip* 6(3):437–446
- Glawdel T, Elbuken C et al (2012a) Droplet formation in microfluidic T-junction generators operating in the transitional regime. I. Experimental observations. *Phys Rev E* 85(1):016322
- Glawdel T, Elbuken C et al (2012b) Droplet formation in microfluidic T-junction generators operating in the transitional regime. II. Modeling. *Phys Rev E* 85(1):016323
- Glawdel T, Elbuken C et al (2011) Passive droplet trafficking at microfluidic junctions under geometric and flow asymmetries. *Lab Chip* 11(22):3774–3784
- Hashimoto M, Shevkoplyas SS et al (2008) Formation of Bubbles and Droplets in Parallel. Coupled Flow-Focusing Geometries. *Small* 4(10):1795–1805
- Korczyk PM, Cybulski O et al (2011) Effects of unsteadiness of the rates of flow on the dynamics of formation of droplets in microfluidic systems. *Lab Chip* 11(1):173–175
- Labrot V, Schindler M et al (2009) Extracting the hydrodynamic resistance of droplets from their behavior in microchannel networks. *Biomicrofluidics* 3:012804
- Li W, Young EWK et al (2008) Simultaneous generation of droplets with different dimensions in parallel integrated microfluidic droplet generators. *Soft Matter* 4(2):258–262
- Malsch D, Gleichmann N et al (2010) Dynamics of droplet formation at T-shaped nozzles with elastic feed lines. *Microfluidics Nanofluidics* 8(4):497–507
- Schindler M, Ajdari A (2008) Droplet traffic in microfluidic networks: A simple model for understanding and designing. *Phys Rev Lett* 100(4):044501
- Sessoms DA, Amon A et al (2010) Complex Dynamics of Droplet Traffic in a Bifurcating Microfluidic Channel: Periodicity, Multistability, and Selection Rules. *Phys Rev Lett* 105(15):154501
- Steegmans MLJ, Schroen C et al (2009) Generalised insights in droplet formation at T-junctions through statistical analysis. *Chem Eng Sci* 64(13):3042–3050
- Sullivan MT, Stone HA (2008) The role of feedback in microfluidic flow-focusing devices. *Philos T R Soc A* 366(1873):2131–2143
- Tetradis-Meris G, Rossetti D et al (2009) Novel Parallel Integration of Microfluidic Device Network for Emulsion Formation. *Ind Eng Chem* 48(19):8881–8889
- van Steijn V, Kreutzer MT et al (2008) Velocity fluctuations of segmented flow in microchannels. *Chem Eng J* 135:S159–S165
- van Steijn V, Kleijn CR et al (2009) Flows around Confined Bubbles and Their Importance in Triggering Pinch-Off. *Phys Rev Lett* 103(21):214501
- van Steijn V, Kleijn CR et al (2010) Predictive model for the size of bubbles and droplets created in microfluidic T-junctions. *Lab Chip* 10(19):2513–2518
- Vanapalli SA, Banpurkar AG et al (2009) Hydrodynamic resistance of single confined moving drops in rectangular microchannels. *Lab Chip* 9(7):982–990
- Ward T, Faivre M et al (2005) Microfluidic flow focusing: drop size and scaling in pressure versus flow-rate-driven pumping. *Electrophoresis* 26(19):3716–3724